VIP Spin Crossover Very Important Paper

Deutsche Ausgabe: DOI: 10.1002/ange.201605418
Internationale Ausgabe: DOI: 10.1002/anie.201605418

Hysteretic Four-Step Spin Crossover within a Three-Dimensional Porous Hofmann-like Material

*John E. Clements, Jason R. Price, Suzanne M. Neville, and Cameron J. Kepert**

Abstract: *Materials that display multiple stepped spin crossover (SCO) transitions with accompanying hysteresis present the opportunity for ternary, quaternary, and quinary electronic switching and data storage but are rare in existence. Herein, we present the first report of a four-step hysteretic SCO framework. Single-crystal structure analysis of a porous 3D Hofmann-like material showed long-range ordering of spin states: HS, $HS_{0.67}LS_{0.33}$, $HS_{0.5}LS_{0.5}$, $HS_{0.33}LS_{0.67}$, and LS. These detailed structural studies provide insight into how multistep SCO materials can be rationally designed through control of host–host and host–guest interactions.*

Advanced materials, in particular those that incorporate multiple properties, are highly sought after for the development of next generation "smart" materials capable of responding to external stimuli in unusual ways. Porous metal–organic frameworks with combined stepped spin crossover (SCO) activity show strong potential in this area as these materials exhibit solid-state switching transitions between high spin (HS, $S=2$) and low spin (LS, $S=0$) Fe^{II} states that are sensitive to changes in interactions with guest molecules.[1] This leads to complex host–guest synergies, whereby external influences that govern the switching process (e.g., temperature, pressure, light) are closely entwined with internal host–guest interactions.[2] For example, the Hofmann-type material $[Fe^{II}(pyrazine)M^{II}(CN)_4]$ ($M^{II}=$ Ni, Pd, Pt) has been shown through magnetic, optical, and guest adsorption/desorption measurements to exhibit pronounced SCO-induced changes to host–guest properties as well as guest-induced changes to SCO.[2a]

Within the realm of SCO materials, those displaying multistepped and multistable hysteretic SCO transitions are emerging as promising candidates for expanded information storage opportunities. For example, we previously reported the porous Hofmann-type material $[Fe(dpsme)Pt(CN)_4]\cdot{}^2/_3$-(dpsme)$\cdot x\,EtOH\cdot y\,H_2O$ (dpsme = 4,4′-di(pyridylthio)methane), which displays the first hysteretic three-step SCO with distinct bi- and tristability, thereby providing access to up to three states at a particular temperature through variation in thermal history.[3] From the few studies of materials that exhibit three or more steps, it is evident that multistepped spin transitions are enabled through cooperative lattice effects, in which elastic (and potentially also electronic) pathways allow the stabilization of states intermediate between HS and LS.[3–4] More explicitly, for multiple intermediates to exist, states with HS fractions other than the more typical $^1/_2$, present for two-step materials ($HS\rightarrow HS_{0.5}LS_{0.5}\rightarrow$ LS), must be stabilized.[5] These fractional changes require that more complex arrangements of SCO centers establish structural ordering, potentially causing significant lattice strain given the mismatch in coordination bond lengths for the LS and HS states; accordingly, to date only a handful of SCO compounds exhibiting more than two steps have been reported, with only a small fraction of these having been structurally characterized in detail.[3,4,6]

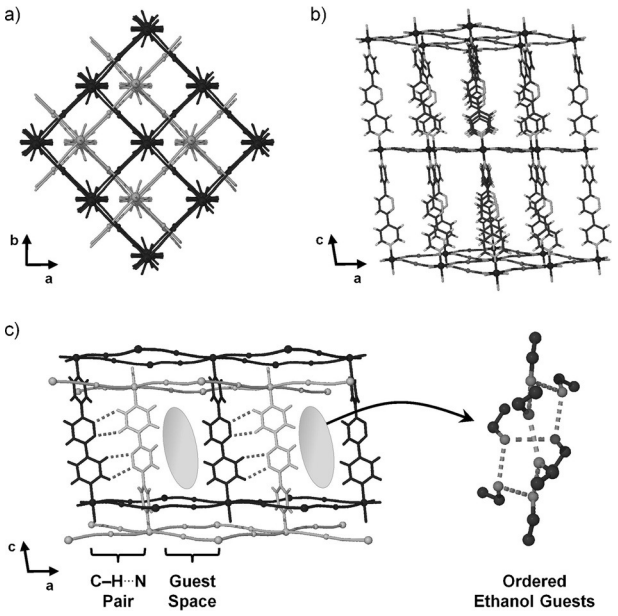

Figure 1. Structural representations of $\mathbf{1^{AS}}$. a) View down the *c* axis, with the two interpenetrating nets shaded differently. b) Perspective view down the *b* axis, with solvent and interpenetration removed for clarity. c) C–H···N interactions between bipydz ligands across interpenetrating nets, with ellipses showing the regions of ordered ethanol molecules (expanded on the right).

Encouraged by our previous findings on the structural and electronic consequences of ligand postsynthetic modification (PSM) within the Hofmann-like material $[Fe^{II}(L)(Au^{I}(CN)_2)_2]\cdot x\,(EtOH)$ from L = 3,6-bis(4-pyridyl)-1,2,4,5-tetrazine (bipytz) to L = 3,6-bis(4-pyridyl)-1,2-diazine (bipydz), we were motivated to compare the structural and SCO

[*] Dr. J. E. Clements, Dr. S. M. Neville, Prof. C. J. Kepert
School of Chemistry, University of Sydney
Sydney, NSW 2006 (Australia)
E-mail: Cameron.kepert@sydney.edu.au
Dr. J. R. Price
Australian Synchrotron Company Limited
800 Blackburn Road, Clayton, VIC 3168 (Australia)

Supporting information for this article can be found under: http://dx.doi.org/10.1002/anie.201605418.

properties of the PSM material $\mathbf{1}^{\mathbf{PSM}}$ to the as-synthesized material produced using the ex situ functionalized ligand bipydz.[7] Slow diffusion of the components ($FeClO_4{\cdot}x\,H_2O$, $KAu(CN)_2$, and bipydz) into ethanol produced crystals of $[Fe^{II}(bipydz)(Au^{I}(CN)_2)_2]{\cdot}4(EtOH)$, $\mathbf{1}^{\mathbf{AS}}$ (AS = as-synthesized), over several weeks. Single-crystal X-ray diffraction (SCXRD) analysis revealed a 3D expanded Hofmann-like network with Fe^{II} centers that are coordinated equatorially by linear dicyanoaurate linkers within the *ab* plane and axially by bipydz ligands along the *c* axis, a topology analogous to that seen in $\mathbf{1}^{\mathbf{PSM}}$. The 3D nets are interpenetrated and are stabilized by aurophilic interactions and ligand–ligand C–H···N interactions between the nets (Figure 1 a, c).

While of the same framework connectivity, pronounced structural differences exist between $\mathbf{1}^{\mathbf{AS}}$ and $\mathbf{1}^{\mathbf{PSM}}$. Most notably, $\mathbf{1}^{\mathbf{AS}}$ contains ordered bipydz ligands that are tilted to foster lateral shifts between highly regular Hofmann-like layers, whereas $\mathbf{1}^{\mathbf{PSM}}$ maintains the untilted ligands and regular alignment of the torsionally compressed layers of its synthetic parent but contains extensive ligand disorder (see the Supporting Information, Figures S4 and S5); each of these distinct arrangements serves to avoid inter-ring ligand C–H···H–C steric clashes whilst achieving favorable inter-ring C–H···N interactions. Despite its interpenetration, $\mathbf{1}^{\mathbf{AS}}$ contains extensive pore volume, with solvent-accessible channels running along the *a* axis (with dimensions of 6×12 Å^2). The ethanol molecules housed within these channels are ordered, interacting with bipydz ligands through C–H···O interactions and with each other by O–H···O hydrogen bonding to form an eight-membered hydrogen-bonding ring; in contrast, the $\mathbf{1}^{\mathbf{PSM}}$ analogue shows no solvent ordering. Thus two distinct polymorphic forms are readily accessible by the synthetic route employed, with $\mathbf{1}^{\mathbf{PSM}}$ retaining the general structure of its higher-symmetry topotactic parent but with ligand disorder, whereas the as-synthesized phase $\mathbf{1}^{\mathbf{AS}}$ establishes a markedly different framework geometry through ligand ordering.

Variable-temperature magnetic susceptibility measurements carried out on bulk crystal samples of $\mathbf{1}^{\mathbf{AS}}$ revealed an abrupt, hysteretic, four-step spin transition of the Fe^{II} sites from HS ($\chi_M T = 3.3$ cm^3 K mol^{-1}) at 250 K to LS ($\chi_M T = 0.2$ cm^3 K mol^{-1}) at 50 K (Figure 2). The fully HS state (HS_1LS_0), $\mathbf{1}^{\mathbf{AS}}$-***i***, is stable upon cooling to 200 K. The transition to $\mathbf{1}^{\mathbf{AS}}$-***ii*** occurs abruptly with cooling below 200 K and corresponds to the conversion of $^1/_3$ of the HS sites to the LS state ($HS_{0.67}LS_{0.33}$). Further cooling sees the stabilization of a 50:50 HS/LS state, $\mathbf{1}^{\mathbf{AS}}$-***iii***, which is present over a 42 K range. The subsequent two steps proceed by an open hysteresis loop $\mathbf{1}^{\mathbf{AS}}$-***iii***↔$\mathbf{1}^{\mathbf{AS}}$-***v***, corresponding to conversion into $HS_{0.33}LS_{0.67}$ and HS_0LS_1 states, respectively. Overall, the transition has increasing thermal hysteresis with each step (3, 6, 20, 22 K). It is possible to traverse the hysteresis gaps at the $\mathbf{1}^{\mathbf{AS}}$-***ii*** and $\mathbf{1}^{\mathbf{AS}}$-***iv*** states (Figure S23), with all states being kinetically stable, whereby holding the temperature constant at each plateau does not result in spin state relaxation (Figure S24).

To confirm that the four-step SCO observed represents the bulk material rather than a mixture of phases, variable-temperature synchrotron powder X-ray diffraction (S-PXRD) measurements were conducted. The evolution of the diffraction peaks with temperature (Figure 3 a) clearly reflects the multistep behavior, indicating that it emanates from a single phase. The unit-cell volumes as determined by Le Bail extraction are in excellent agreement with the bulk magnetic data, with all four steps and the corresponding five magnetic states being clearly present (Figure 3 b). The precise

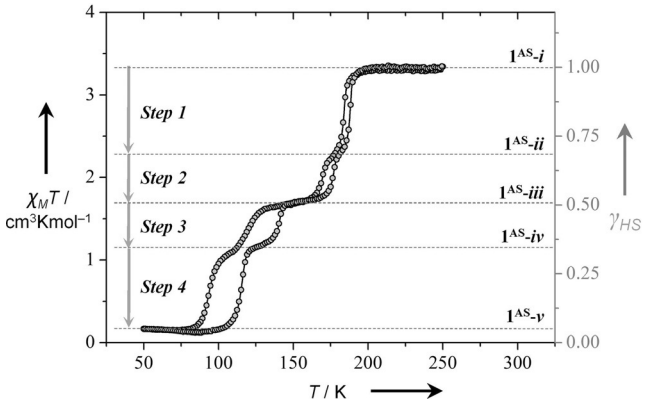

Figure 2. Variable-temperature magnetic susceptibility data for $\mathbf{1}^{\mathbf{AS}}$, with states and steps labeled. Dashed lines at state HS fractions (γ_{HS}) are provided as a guide.

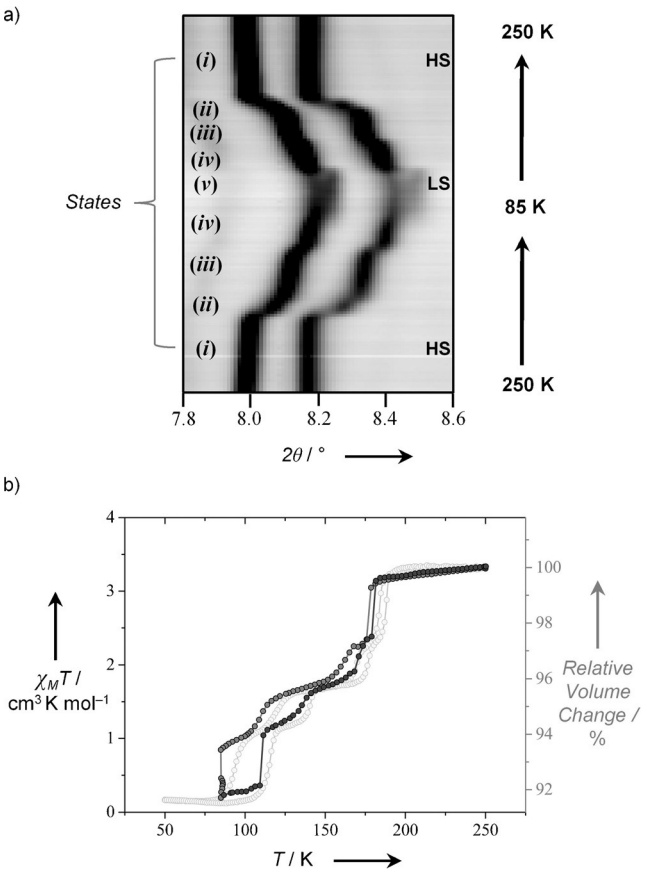

Figure 3. a) Variable-temperature S-PXRD of $\mathbf{1}^{\mathbf{AS}}$ upon cooling and heating between 250 and 85 K, showing changes to the (220) (left) and (22$\bar{2}$) (right) reflections. b) S-PXRD unit cell volumes of **1** upon cooling (●) and heating (●), overlaid onto the bulk magnetic susceptibility (○).

structural changes were subsequently monitored by SCXRD at multiple temperatures (250, 175, 140, 120, and 90 K), which constitute each of the five states, revealing a series of SCO-induced phase transitions. The HS and LS spin-state structures, $\mathbf{1}^{\mathbf{AS}}$-***i*** and $\mathbf{1}^{\mathbf{AS}}$-***v***, adopt the same symmetry and lattice settings. With respect to these, transitions to $\mathbf{1}^{\mathbf{AS}}$-***ii*** and $\mathbf{1}^{\mathbf{AS}}$-***iv*** experience a commensurate modulation with tripling of the Hofmann layer periodicity, and $\mathbf{1}^{\mathbf{AS}}$-***iii*** is distinct in undergoing a symmetry lowering within the parent cell. The complete series and corresponding spin-state ordering are schematically shown in Figure 4, with full information provided in Table S1.

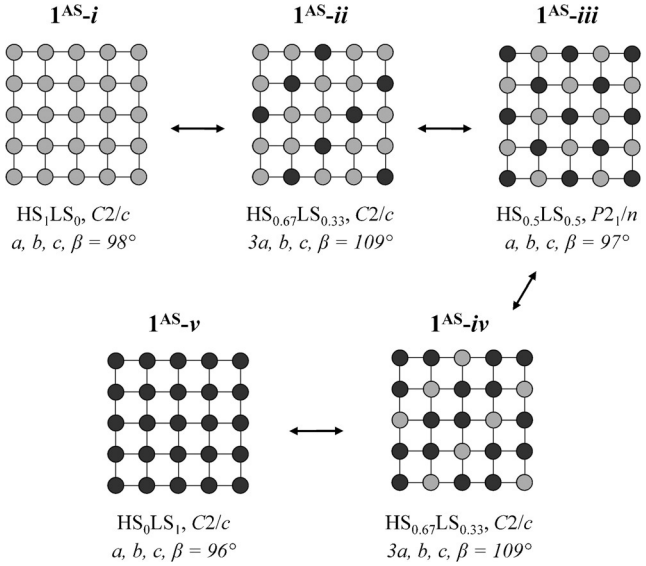

Figure 4. Table and graphical representation of the spin-state ordering that occurs in each state of $\mathbf{1}^{\mathbf{AS}}$ upon cooling/warming. Fe^{II} sites drawn as circles (● = HS site, ● = LS site). $Au^{I}(CN)_2^-$ linkers are shown as lines.

The LS phase, $\mathbf{1}^{\mathbf{AS}}$-***v***, adopts a monoclinic *C*-centered lattice in the *C2/c* space group with one crystallographically unique Fe^{II} site with Fe–N distances typical of LS Fe^{II} ($\langle d_{Fe-N}\rangle = 1.97$ Å). The transition to $\mathbf{1}^{\mathbf{AS}}$-***iv*** on warming involves the formation of an enlarged supercell in which tripling of the unit-cell volume accompanies the formation of three crystallographically distinct Fe^{II} sites, two LS ($\langle d_{Fe-N}\rangle =$ 1.98 Å each) and one HS (2.12 Å); comparable levels of octahedral distortion are seen at each site (Table S7). These sites arrange themselves in diagonal stripes within the Hofmann-like layer (Figure 4). Further warming produces $\mathbf{1}^{\mathbf{AS}}$-***iii***, leading to a loss of the tripled supercell and a return to the parent unit cell, now without *C* centering. Two distinct Fe^{II} sites are thus generated, one HS ($\langle d_{Fe-N}\rangle = 2.15$ Å) and the other LS (1.97 Å), leading to a change in periodicity of the HS/LS layer stripes such that they now adopt a checkerboard arrangement (Figure 4). Further warming induces conversion into $\mathbf{1}^{\mathbf{AS}}$-***ii***, which reintroduces the tripled supercell. Full quantitative refinement of this state was hindered by the very narrow temperature range over which it is stable, with slight variations in temperature during data collection perturbing the spin and structural state, resulting in unreliable intensities for the superstructure peaks. We inferred the highly correlated structure in part from constrained refinement attempts and from comparison with $\mathbf{1}^{\mathbf{AS}}$-***iv*** (Figures S11 and S16). Upon further warming, the fully HS state, $\mathbf{1}^{\mathbf{AS}}$-***i***, is generated, re-establishing the parent symmetry and cell, in which only one HS Fe^{II} site is found ($\langle d_{Fe-N}\rangle = 2.19$ Å).

A striking feature of the various observed forms of spin-state patterning is that they occur with 3D ordering, that is, registry is achieved not just within each Hofmann-like layer in the *ab* plane, but also along the pillar direction (*c* axis); this has accordingly enabled the detailed analysis of these states by Bragg diffraction methods. More notably, the 3D patterning of one network occurs in registry with that of its interpenetrated partner, indicating that the interframework aurophilic and hydrogen-bonding interactions (and potentially also those mediated through the ethanol guests) are of sufficient strength to lead to full crystallographic ordering (Figure S3). We have previously reported a similar feature in a two-step system consisting of interpenetrated 2D nets,[1c] and believe that crystal packing effects associated with weaker interactions are at least in part responsible for the stabilization of the intermediate lattice spin states witnessed here. Indeed, whereas states $\mathbf{1}^{\mathbf{AS}}$-***i***, $\mathbf{1}^{\mathbf{AS}}$-***iii***, and $\mathbf{1}^{\mathbf{AS}}$-***v*** adopt regular, unstrained framework geometries, with $\mathbf{1}^{\mathbf{AS}}$-***iii*** existing as a "3D checkerboard" in which HS and LS sites alternate in all directions, states $\mathbf{1}^{\mathbf{AS}}$–***ii*** and $\mathbf{1}^{\mathbf{AS}}$-***iv*** necessitate some degree of framework strain, relief of which appears likely to be stabilized by the weak interframework and guest-mediated interactions.

We then turned our attention to the various intermolecular interactions present and their likely role in influencing the multistep SCO behavior.[8] Many interactions adjust significantly through the multistage transformation from $\mathbf{1}^{\mathbf{AS}}$-***i*** to $\mathbf{1}^{\mathbf{AS}}$-***v***. Overall, the aurophilic and C–H···N interactions are shortened incrementally through each of the steps. Concomitant with these changes are deviations to the framework geometry; notably, pyridyl–diazine ring torsions increase and the Fe-N-C angles straighten with progressive conversion into the LS state. Curiously, there are no obvious changes to the guest molecule positions across all states, with the eight-membered hydrogen-bonding ring maintaining C–H···O interactions with bipydz and O···O distances below 3 Å (Figure 1c). However, there is the possibility that the hydrogen atoms that form the links in the chain can change direction and/or differ between unit cells, suggesting that their relative arrangements may have a very subtle influence over the spin state of the material; this hypothesis is consistent with the fact that the stepped and hysteretic behavior is lost upon guest removal (see Figure S22). When intermolecular interactions and the resulting SCO of $\mathbf{1}^{\mathbf{PSM}}$ and $\mathbf{1}^{\mathbf{AS}}$ are compared, the former can be considered as a "kinetic" product in which the lack of regioselectivity of the modification reaction prevents the framework translation to optimize C–H···N interactions, leaving the ligands and guests disordered. In turn, the latter can be considered the "thermodynamic" product that has optimized ligand and guest positions. These subtle changes between polymorphs clearly affect the interplay between structure and magnetic behavior; in $\mathbf{1}^{\mathbf{PSM}}$ and its

1,2,4,5-tetrazine precursor (both single-step SCO), the FeN_6 octahedron displays a reversal of the expected changes in distortion across the spin transition and the lattice undergoes a "scissor motion", whereby the *a* axis expands and the *b* axis contracts.[7] These effects are not present in the four-step SCO of $\mathbf{1}^{\mathbf{AS}}$, suggesting that interframework, framework–guest interactions and framework deformation play a critical role in the stabilization of the intermediate spin states. Specifically, it appears that the asymmetric hydrogen-bonding pairs in $\mathbf{1}^{\mathbf{AS}}$ may serve to stabilize the intermediate states within the multistep transition, suggesting in turn that regimes that involve guest molecules of type H···H···G···H···H···G··· (where H = host, G = guest) are a synthetic target for developing new multistep SCO materials.

In considering the full progressive conversion through the various ordered states upon cooling/warming, an interesting implication is that individual Fe^{II} sites must necessarily be dynamic in their spin state rather than becoming fixed once switched. This feature is exemplified in Figure 4, which shows how the mismatch in the periodicities of $\mathbf{1}^{\mathbf{AS}}$-*ii*, $\mathbf{1}^{\mathbf{AS}}$-*iii*, and $\mathbf{1}^{\mathbf{AS}}$-*iv* induces individual sites to undergo HS→LS→HS→LS conversion upon cooling, such that local reverse SCO (RSCO) from LS to HS occurs despite a net decrease in magnetic moment for the bulk material; this behavior is distinct from bulk RSCO, as has been seen, for example, in liquid crystalline Co^{II} SCO systems,[9] in which electronically unfavorable spin switching is driven by the competing energetics of non-electronic structural transitions. This novel feature confirms that the thermal hystereses observed in steps 2 and 3 (see Figure 2) are derived from bulk dynamic lattice effects rather than, for example, a rigid freezing in of local framework/guest conformation. A corollary of this is that 3D "spin-state concentration waves" of HS and LS sites within each lattice state are likely highly mobile, akin to charge density waves in electronically delocalized systems and presumably similarly susceptible to becoming disrupted and locked onto crystal defects, particularly if of lower dimension.[10] Communication of these waves throughout the lattice may be responsible for the intolerance of particular HS/LS ratios and aperiodic orderings, as was observed recently in a three-step transition.[4c]

To conclude, the synthesis and structural properties of the first four-step SCO framework material have been described. From just one unique Fe^{II} site in the HS state, the compound changes lattice symmetry and periodicity through multiple steps to incorporate new, inequivalent Fe^{II} sites of varying integral HS fraction. The stabilization of these intermediate states is broadly analogous to the observation of discrete mixed-compositional line phases in highly cooperative solids such as metal oxides, in which doping with ions of varying radii commonly leads to phase separation between line phases of integral composition rather than the formation of solid solutions. Here, this doping of inequivalent ions is achieved thermally through the dynamic conversion of the larger HS Fe^{II} centers into smaller LS sites, such that distinct line phases of composition $Fe(HS)_{1-x}Fe(LS)_x$ ($x = 0$, $^1/_3$, $^1/_2$, $^2/_3$, 1) are stabilized and exhibit 3D crystallographic ordering. As each individual state is kinetically stable and accessible through thermal control, the material presents a very rare example where five distinct electronic states $\mathbf{1}^{\mathbf{AS}}$-*i*→$\mathbf{1}^{\mathbf{AS}}$-*v* can be accessed. Through comparison of the as-synthesized material ($\mathbf{1}^{\mathbf{AS}}$) with the polymorph generated by an alternate synthetic route ($\mathbf{1}^{\mathbf{PSM}}$), important structure–property relationships emerged, highlighting the fundamentally sensitive nature of SCO and how it may be exploited for its sensitivity. From a general outlook, the incorporation of guest-sensitive hydrogen-bonding host–host pairs could afford a design pathway to multistep SCO behavior, providing interesting potential for the development of highly sensitive and responsive materials.

Experimental Section

Crystals of $\mathbf{1}^{\mathbf{AS}}$ were obtained by the slow diffusion of ethanol solutions of bipydz (9 mg, 0.038 mmol), $KAu(CN)_2$ (22 mg, 0.076 mmol), and $FeClO_4 \cdot x\,H_2O$ (10 mg, 0.039 mmol). Yellow crystals formed over several weeks. CCDC 1482906 ($\mathbf{1}^{\mathbf{AS}}$-*v*), 1482907 ($\mathbf{1}^{\mathbf{AS}}$-*i*), 1482908 ($\mathbf{1}^{\mathbf{AS}}$-*iv*), and 1482909 ($\mathbf{1}^{\mathbf{AS}}$-*iii*) contain the supplementary crystallographic data for this paper. These data can be obtained free of charge from The Cambridge Crystallographic Data Centre.

Acknowledgements

This work was supported by research and fellowship funding from the Australian Research Council (C.J.K., S.M.N.) and a World Scholar Award (J.E.C.). We acknowledge travel funding provided by the International Synchrotron Access Program (ISAP) managed by the Australian Synchrotron and funded by the Australian Government. Use of the Advanced Photon Source (APS) at Argonne National Laboratory was supported by the U.S. Department of Energy, Office of Science, Office of Basic Energy Sciences (DE-AC02-06CH11357). We thank Dr G. J. Halder for assistance at the APS beamline.

Keywords: host–guest systems · metal–organic frameworks · microporous materials · spin crossover · supramolecular chemistry

How to cite: *Angew. Chem. Int. Ed.* **2016**, *55*, 15105–15109
Angew. Chem. **2016**, *128*, 15329–15333

[1] a) G. J. Halder, C. J. Kepert, B. Moubaraki, K. S. Murray, J. D. Cashion, *Science* **2002**, *298*, 1762–1765; b) X. Bao, H. J. Shepherd, L. Salmon, G. Molnár, M.-L. Tong, A. Bousseksou, *Angew. Chem.* **2013**, *125*, 1236–1240; c) G. J. Halder, K. W. Chapman, S. M. Neville, B. Moubaraki, K. S. Murray, J.-F. Létard, C. J. Kepert, *J. Am. Chem. Soc.* **2008**, *130*, 17552–17562; d) J.-Y. Li, Y.-C. Chen, Z.-M. Zhang, W. Liu, Z.-P. Ni, M.-L. Tong, *Chem. Eur. J.* **2015**, *21*, 1645–1651; e) C. Bartual-Murgui, N. A. Ortega-Villar, H. J. Shepherd, M. C. Muñoz, L. Salmon, G. Molnar, A. Bousseksou, J. A. Real, *J. Mater. Chem.* **2011**, *21*, 7217–7222.

[2] a) P. D. Southon, L. Liu, E. A. Fellows, D. J. Price, G. J. Halder, K. W. Chapman, B. Moubaraki, K. S. Murray, J. F. Létard, C. J. Kepert, *J. Am. Chem. Soc.* **2009**, *131*, 10998–11009; b) V. Niel, J. M. Martinez-Agudo, M. C. Muñoz, A. B. Gaspar, J. A. Real, *Inorg. Chem.* **2001**, *40*, 3838–3839; c) M. Ohba, K. Yoneda, G. Agustí, M. C. Muñoz, A. B. Gaspar, J. A. Real, M. Yamasaki, H. Ando, Y. Nakao, S. Sakaki, S. Kitagawa, *Angew. Chem. Int. Ed.* **2009**, *48*, 4767–4771; *Angew. Chem.* **2009**, *121*, 4861–4865; d) R.

Ohtani, K. Yoneda, S. Furukawa, N. Horike, S. Kitagawa, A. B. Gaspar, M. Carmen Muñoz, J. A. Real, M. Ohba, *J. Am. Chem. Soc.* **2011**, *133*, 8600 – 8605; e) S. Bonhommeau, G. Molnár, A. Galet, A. Zwick, J.-A. Real, J. J. McGarvey, A. Bousseksou, *Angew. Chem. Int. Ed.* **2005**, *44*, 4069 – 4073; *Angew. Chem.* **2005**, *117*, 4137 – 4141.

[3] N. F. Sciortino, K. R. Scherl-Gruenwald, G. Chastanet, G. J. Halder, K. W. Chapman, J.-F. Létard, C. J. Kepert, *Angew. Chem. Int. Ed.* **2012**, *51*, 10154 – 10158; *Angew. Chem.* **2012**, *124*, 10301 – 10305.

[4] a) M. Nihei, H. Tahira, N. Takahashi, Y. Otake, Y. Yamamura, K. Saito, H. Oshio, *J. Am. Chem. Soc.* **2010**, *132*, 3553 – 3560; b) Z.-Y. Li, J.-W. Dai, Y. Shiota, K. Yoshizawa, S. Kanegawa, O. Sato, *Chem. Eur. J.* **2013**, *19*, 12948 – 12952; c) E. Trzop, D. Zhang, L. Piñeiro-Lopez, F. J. Valverde-Muñoz, M. C. Muñoz, L. Palatinus, L. Guerin, H. Cailleau, J. A. Real, E. Collet, *Angew. Chem. Int. Ed.* **2016**, *55*, 8675 – 8679; *Angew. Chem.* **2016**, *128*, 8817 – 8821.

[5] a) T. Matsumoto, G. N. Newton, T. Shiga, S. Hayami, Y. Matsui, H. Okamoto, R. Kumai, Y. Murakami, H. Oshio, *Nat. Commun.* **2014**, *5*, 3865; b) J. Klingele, D. Kaase, M. H. Klingele, J. Lach, S. Demeshko, *Dalton Trans.* **2010**, *39*, 1689 – 1691; c) Y. M. Klein, N. F. Sciortino, F. Ragon, C. E. Housecroft, C. J. Kepert, S. M. Neville, *Chem. Commun.* **2014**, *50*, 3838 – 3840; d) B. J. C. Vieira, J. T. Coutinho, I. C. Santos, L. C. J. Pereira, J. C. Waerenborgh, V. da Gama, *Inorg. Chem.* **2013**, *52*, 3845 – 3850; e) J.-B. Lin, W. Xue, B.-Y. Wang, J. Tao, W.-X. Zhang, J.-P. Zhang, X.-M. Chen, *Inorg. Chem.* **2012**, *51*, 9423 – 9430; f) K. Bhar, S. Khan, J. S. Costa, J. Ribas, O. Roubeau, P. Mitra, B. K. Ghosh, *Angew. Chem.* **2012**, *124*, 2184 – 2187; g) N. Ortega-Villar, M. C. Muñoz, J. A. Real, *Magnetochemistry* **2016**, *2*, 16.

[6] a) T. Kosone, I. Tomori, C. Kanadani, T. Saito, T. Mochida, T. Kitazawa, *Dalton Trans.* **2010**, *39*, 1719 – 1721; b) K. Yoshida, D. Akahoshi, T. Kawasaki, T. Saito, T. Kitazawa, *Polyhedron* **2013**, *66*, 252 – 256.

[7] J. E. Clements, J. R. Price, S. M. Neville, C. J. Kepert, *Angew. Chem. Int. Ed.* **2014**, *53*, 10164 – 10168; *Angew. Chem.* **2014**, *126*, 10328 – 10332.

[8] M. A. Halcrow, *Chem. Soc. Rev.* **2011**, *40*, 4119 – 4141.

[9] S. Hayami, Y. Shigeyoshi, M. Akita, K. Inoue, K. Kato, K. Osaka, M. Takata, R. Kawajiri, T. Mitani, Y. Maeda, *Angew. Chem. Int. Ed.* **2005**, *44*, 4899 – 4903; *Angew. Chem.* **2005**, *117*, 4977 – 4981.

[10] a) M. R. Bryce, *J. Mater. Chem.* **1995**, *5*, 1481 – 1496; b) E. Collet, H. Watanabe, N. Bréfuel, L. Palatinus, L. Roudaut, L. Toupet, K. Tanaka, J.-P. Tuchagues, P. Fertey, S. Ravy, B. Toudic, H. Cailleau, *Phys. Rev. Lett.* **2012**, *109*, 257206; c) H. Watanabe, K. Tanaka, N. Bréfuel, H. Cailleau, J.-F. Létard, S. Ravy, P. Fertey, M. Nishino, S. Miyashita, E. Collet, *Phys. Rev. B* **2016**, *93*, 014419.

Received: June 3, 2016
Published online: October 21, 2016

